Vibrational and thermodynamic properties of wadsleyite: A density functional study

Zhongqing Wu[1] and Renata M. Wentzcovitch[1]

Received 8 March 2007; revised 3 July 2007; accepted 16 August 2007; published 8 December 2007.

[1] The vibrational properties of Mg_2SiO_4 wadsleyite have been calculated over a wide pressure range using density functional perturbation theory (DFPT). Both the normal mode frequencies and their volume dependences are consistent with the available Raman and infrared data. We provide detailed information about vibrational properties that are still not experimentally available. The vibrational density of states (vDOS) is used to calculate the Helmholtz free energy within the quasi-harmonic approximation (QHA) and other thermodynamic quantities without further approximations. The extensive and successful comparisons with experiments demonstrate once more that the QHA combined with first principles vDOSs can provide accurate thermodynamic properties of minerals over the large pressure-temperature regime relevant for the Earth.

Citation: Wu, Z., and R. M. Wentzcovitch (2007), Vibrational and thermodynamic properties of wadsleyite: A density functional study, *J. Geophys. Res.*, *112*, B12202, doi:10.1029/2007JB005036.

1. Introduction

[2] Minerals with composition $(Mg,Fe)_2SiO_4$ are the most abundant ones in Earth's upper mantle and transition zone. There are three polymorphs with this composition: olivine (α), wadsleyite (β), and ringwoodite (γ), the latter being a spinel phase. These phases are stable at different depths, with α, β, and γ' stability pressure fields increasing with pressure in this order. The seismic discontinues near 410, 520 and 660 km depths in the mantle have been attributed to the α-β and β-γ transformations, and to the dissociation of $(Mg,Fe)_2SiO_4$ into perovskite $(Mg,Fe)SiO_3$ and ferropericlase (Mg,Fe)O, respectively [*Ringwood*, 1975]. The β and γ phases are also likely to play important roles in the global hydrogen cycle [*Smyth*, 1987; *Kohlstedt et al.*, 1996]. Theoretical and experimental investigations have shown that wadsleyite can incorporate up to 3.3 wt % H_2O in its crystal structure [*Smyth*, 1987, 1994; *Inoue et al.*, 1995; *Kudoh et al.*, 1996], suggesting that the the transition zone may be a major water reservoir in the Earth's interior. Which site H occupies and how the presence of water influences phase relations and physical properties is a topic of active current research [*Jacobsen et al.*, 2005; *Kohn et al.*, 2002; *Ohtani and Litasov*, 2006]. Knowledge of the physical properties of these polymorphs is very important to clarify the nature and properties of Earth's mantle, particularly the transition zone.

[3] In succession to the recent density functional study of the vibrational and thermodynamic properties of forsterite (α) [*Li et al.*, 2007] and ringwoodite (γ) [*Yu and Wentzcovitch*, 2006] phases, we focus our attention on wadsleyite (β). The vibrational properties of the β phase have been studied extensively by Raman and infrared spectroscopy [*Akaogi et al.*, 1984; *Williams et al.*, 1986; *Reynard et al.*, 1996; *Mernagh and Liu*, 1996; *Kleppe et al.*, 2001; *Cynn and Hofmeister*, 1994; *Chopelas*, 1991]. These vibrational modes have been used in the past to investigate a number of macroscopic properties such as the specific heat, entropy, and phases relations [*Akaogi et al.*, 1984; *Chopelas et al.*, 1994; *Reynard et al.*, 1996]. However, knowledge of vibrational and thermodynamic properties of wadsleyite is still very limited. Only some of the Raman and infrared modes have been observed. The detailed vibrational density of state that is necessary to calculate accurately thermodynamic properties is still unavailable, particularly at transition zone pressures. Unambiguous symmetry assignments are still absent for observed modes.

[4] Few theoretical studies have been carried out on the properties of wadsleyite at simultaneous high temperatures and pressures. The structure and elasticity of wadsleyite have been investigated by *Matsui* [1999] using molecular dynamic simulation and by *Kiefer et al.* [2001] by first principles methods. However, up to now, there has been no first principle theoretical work on lattice dynamics and thermodynamic properties of wadsleyite. Here we report phonon calculations of wadsleyite over the range of pressures relevant for the transition zone, using density functional perturbation theory (DFPT) [*Baroni et al.*, 2001]. Phonon dispersion, Raman and infrared mode frequencies, and thermodynamic quantities such as thermal expansivity, heat capacity, and entropy are derived from these calculations and compared with experiments.

2. Method

[5] The techniques and the details of calculation used here are similar to those used in previous work [*Wentzcovitch et al.*, 2004]. Computations were performed using the local

[1]Department of Chemical Engineering and Materials Science and Minnesota Supercomputing Institute, University of Minnesota-Twin Cities, Minneapolis, Minnesota, USA.

0148-0227/07/2007JB005036$09.00

Table 1. Frequencies, Symmetries, and Mode Grüneisen Parameters for the Raman Modes of Wadsleyite

This Calculation (Raman)			*Chopelas* [1991]		*Akaogi et al.*	*McMillan and Akaogi* [1987]	*Reynard et al.*
ν_i, cm^{-1}	Symmetry	γ_i	ν_i, cm^{-1}	γ_i	[1984] ν_i, cm^{-1}	ν_i, cm^{-1}	[1996] ν_i, cm^{-1}
			86				
			143				
			146				
200.8	B_{2g}	.60	199				
230.4	B_{1g}	1.69	214	1.7	213		
231.8	B_{3g}	1.34	231	1.25		230	231
263.5	B_{1g}	1.66	252	0.806			
267.3	A_g	1.48	262	1.19		268	262
269.5	B_{2g}	1.04	273	0.88			
274.7	B_{3g}	.69	279	0.628	280		
285.2	A_g	1.18	288	0.779			
296.5	B_{1g}	1.18	297			298	
302.6	B_{3g}	1.59	311	0.887	307		
333.6	B_{2g}	1.66	326	1.59		328	
344.2	A_g	1.34	341	1.36		340	341
359.7	B_{1g}	1.34					
361.3	B_{3g}	1.41	360				
367.0	B_{2g}	1.45	370	0.74		368	
385.9	B_{1g}	1.82	382	1.58			
400.1	B_{2g}	1.82	398	1.37		400	398
401.1	B_{3g}	1.62					
405.6	A_g	1.58			408		
424.4	A_g	1.39					
425.0	B_{3g}	1.08	426	0.972		425	426
448.1	B_{1g}	.94	443	1.35		443	443
454.6	A_g	1.29	460		460		
481.7	B_{3g}	.96					
483.9	B_{2g}	.92	491	0.686		489	
543.5	B_{3g}	1.34			528		
556.8	A_g	1.32	553	1.34		551	553
564.1	B_{2g}	.75	580	0.531	570		
577.9	B_{3g}	1.02	585	1.04	588	584	585
607.2	A_g	.77	620	0.689		620	620
624.6	B_{2g}	1.51	610				
711.8	A_g	0.91	723	0.804		723	723
785.8	B_{3g}	1.16	778	1.07		778	778
828.7	B_{3g}	.92	812		836		
890.6	B_{1g}	1.05	845	0.811	850	842	
894.7	A_g	1.02	885		898		885
910.5	A_g	.91	919	0.833	919	918	918
913.5	B_{2g}	.99	949		940		
934.8	B_{3g}	.98	965				
			1020			1100	

density approximation (LDA) [*Perdew and Zunger*, 1981]. The pseudopotential for magnesium was generate by the method of von Barth and Car [*Karki et al.*, 1999], while those for oxygen and silicon were generated by the method of *Troullier and Martins* [1991]. The plane wave cutoff energy is 70 Ry. Brillouin zone summations over electronic states were performed over 4 special k points. Structural optimizations were achieved using damped variable cell shape molecular dynamics [*Wentzcovitch*, 1993]. For each fully optimized structure, dynamical matrices were computed on $2 \times 2 \times 2$ q mesh using density functional perturbation theory (DFPT) [*Baroni et al.*, 2001] and then interpolated in a regular $9 \times 9 \times 9$ q mesh to obtain the vibrational density of state.

3. Vibrational Properties

[6] Wadsleyite has orthorhombic structure with space group *Immm*. It has 4 formula units (28 atoms) per primitive cell. The 84 normal modes at the Brillouin zone center include 3 acoustic modes and 81 optical modes, which may be divided by symmetry as

$$T = 11A_g(R) + 7B_{1g}(R) + 9B_{2g}(R) + 12B_{3g}(R) + 7A_u + 13B_{1u}(IR) + 12B_{2u}(IR) + 10B_{3u}(IR), \quad (1)$$

where R and IR denote Raman and infrared active modes, respectively. There are 35 infrared active and 39 Raman active modes.

[7] Raman and infrared mode frequencies are listed in Tables 1 and 2, respectively. In general, mode symmetries are useful for comparisons between calculated and experimental mode frequencies. However, modes' symmetries are still unknown for most observed modes of wadsleyite. Excellent agreement between first principles predictions and experimental observations of mode frequencies has been shown in many investigations [*Baroni et al.*, 2001; *Karki et al.*, 1999; *Karki and Wentzcovitch*, 2003; *Yu and Wentzcovitch*, 2006, *Li et al.*, 2007]. Therefore our assign-

Table 2. Frequencies, Symmetries and Mode Grüneisen Parameters for the Infrared Modes of Wadsleyite

This Calculation (IR)			*Akaogi et al.* [1984]	*Williams et al.* [1986]		*Cynn and Hofmeister* [1994]	
ν_i, cm^{-1}	Symmetry	γ_i	ν_i, cm^{-1}	ν_i, cm^{-1}	γ_i	ν_i, cm^{-1}	γ_i
190.7	B_{3u}	1.24	188			192	0.41
216.3	B_{2u}	1.47	208			212	0.15
251.9	B_{3u}	.17	266			260	0
267.4	B_{1u}	1.33					
284.7	B_{2u}	1.30	288				
295.5	B_{3u}	1.26					
299.6	B_{1u}	1.41					
313.4	B_{2u}	.84	316				
331.6	B_{3u}	1.62	326	326	1.43		
354.3	B_{1u}	1.58	345				
358.9	B_{2u}	1.44					
359.3	B_{3u}	1.40	359	359	1.41		
359.7	B_{1u}	1.37					
380.3	B_{1u}	1.75	381	381	1.87		
410.6	B_{3u}	1.51					
427.1	B_{2u}	1.50	422	425	1.53		
430.6	B_{1u}	1.54					
455.2	B_{2u}	1.20					
462.2	B_{2u}	1.05					
469.4	B_{1u}	1.32					
488.4	B_{3u}	1.26	485	485	1.21	478	0.96
498.2	B_{1u}	1.11				505	0.52
514.0	B_{2u}	1.07	520	519	1.20	519	0.93
535.1	B_{3u}	1.25					
551.0	B_{3u}	1.18					
552.6	B_{1u}	1.23	550	550	1.59	551	1.13
586.7	B_{1u}	1.09	595	597	1.11	599	0.8
590.3	B_{2u}	1.26	645				
698.7	B_{1u}	1.16	700	700	1.17	700	1.0
794.0	B_{2u}	1.14					
832.6	B_{2u}	.94	811	811	1.11	817	0.82
871.9	B_{1u}	.98	855			837	1.0
909.7	B_{1u}	.93	910			917	0.77
917.6	B_{3u}	.96	945	938	0.90	945	0.90
946.7	B_{2u}	.94	985			975	1.13

ment of symmetries to the experimentally observed modes was made by comparing those frequencies to the calculated ones and should be accurate in the majority of cases. The assignments are listed in Tables 1 and 2. As shown below, the assignments are also supported by comparing the volume dependence of the mode frequencies (mode Grüneisen parameter). Our calculated frequencies agree well with the experimental observations [*Akaogi et al.*, 1984; *McMillan and Akaogi*, 1987; *Williams et al.*, 1986; *Reynard et al.*, 1996; *Cynn and Hofmeister*, 1994; *Chopelas*, 1991]. The Raman results between 200 and 1000 cm^{-1} are very consistent with *Chopelas*' [1991] measurements. The relative difference in frequencies for most Raman modes is less than 2%. Only 4 mode frequencies differ more than 3%, where the largest difference is ~5% for the mode with frequency 890 cm^{-1} (the experimental result is 845 cm^{-1}). Similar agreement between measured and calculated frequencies can also be found for infrared modes [*Akaogi et al.*, 1984; *Williams et al.*, 1986; *Cynn and Hofmeister*, 1994]. The assignments are also supported by the simultaneous agreement between mode Grüneisen parameters $\gamma_i = -d\ln\nu_i/d\ln V$ [*Williams et al.*, 1986; *Cynn and Hofmeister*, 1994; *Chopelas*, 1991]. The γ_i of the infrared mode with frequency 251.9 cm^{-1} is particular small compared to those of all other 80 optical modes. Interestingly, *Cynn and Hofmeister* [1994] also observed an infrared mode frequency nearly volume-independent at 260 cm^{-1}.

[8] There are two kinds of polyhedra in Mg_2SiO_4, SiO_4 tetrahedra and MgO_6 octahedra. In the β phase, SiO_4 tetrahedra are linked in pairs by a corner to form a Si_2O_7 unit; γ_i of the modes with $\nu_i > 700$ cm^{-1}, are significantly smaller than γ_is of the majority of modes with lower frequencies. These modes consist mainly of vibrations of the Si_2O_7 unit keeping magnesium nearly stationary. This is indicated in Table 3 where the amplitude of atomic displacements involved in all vibrational modes is given. The smaller γ_is of these modes indicate that the Si_2O_7 unit is relatively incompressible compared to the MgO_6 unit. This has already been pointed out by experiments [*Hazen et al.*, 2000] and by previous first principles calculations [*Kiefer et al.*, 2001]. It has also been found in olivine [*Hazen*, 1976]. The Si_2O_7 unit can be regarded as two SiO_3 groups connected by a Si-O-Si bridge. We finish the assignments of high-frequency modes by specifying the motion of the SiO_3 group and of the Si-O-Si bridge, respectively, in Table 3. Besides the O-Si bond stretching and Si-O-Si bridge bending, we also found Si-O-Si bridge libration in some modes. Vibrations of the SiO_3 terminal group include stretching and bending. The asymmetric stretches generally have higher frequencies than their symmetric counterparts (see Table 3). Figure 1 shows the atomic displacements for the Si_2O_7 groups involved in these high-energy vibrations. For clarity, displacements have been enlarged uniformly about 4 times. For simplicity only one of the two Si_2O_7

Table 3. Amplitude of Atomic Displacements of Silicon and Three Nonequivalent Magnesium in the Normal Modes at the Γ Point of the Brillouin Zone[a]

ν_i, cm^{-1}	Si, au	Mg1, au	Mg2, au	Mg3, au	Assignment	
					This Work	Experiment
0	0.19	0.19	0.19	0.19		
0	0.19	0.19	0.19	0.19		
0	0.19	0.19	0.19	0.19		
190.7	0.04	0.19	0.17	0.38	Mg	
200.8	0.2	0	0.44	0.03	Si + Mg	
212.7	0.17	0.4	0	0.12	Si + Mg	
216.3	0.06	0.39	0.18	0.28	Mg	
230.4	0.03	0	0	0.43	Mg	
231.8	0.27	0	0.19	0.14	Si + Mg	Mg[c]
251.9	0.09	0.07	0.21	0.18	Mg	
263.5	0.23	0	0	0.17	Si + Mg	
267.3	0.27	0	0.07	0.01		
267.4	0.14	0.34	0.04	0.17	Si + Mg	
269.5	0.13	0	0.09	0.08	Si + Mg	
274.7	0.25	0	0.11	0.19	Si + Mg	
284.7	0.27	0.16	0.11	0.03	Si + Mg	
284.8	0.14	0.04	0	0.38	Si + Mg	
285.2	0.11	0	0.49	0.13	Si + Mg	
295.5	0.07	0.37	0.45	0.18	Mg	
296.5	0.04	0	0	0.25	Mg	
299.6	0.04	0.49	0.36	0.06	Mg	
302.6	0.14	0	0.27	0.32	Si + Mg	
313.4	0.23	0.41	0.34	0.02	Si + Mg	
331.6	0.07	0.04	0.13	0.24	Mg	
333.6	0.04	0	0.19	0.25	Mg	
344.2	0.07	0	0.08	0.04	Mg + SI	
354.3	0.2	0.26	0.33	0.23	Si + Mg	
358.9	0.09	0.3	0.16	0.22	Mg	
359.3	0.05	0.17	0.06	0.2	Mg	
359.7	0.08	0.3	0.05	0.21	Mg	
359.7	0.06	0	0	0.02		
361.3	0.09	0	0.39	0.23	Mg	
367.0	0.01	0	0.1	0.31	Mg	
372.1	0.11	0.19	0	0.23	Si + Mg	
380.3	0.13	0.21	0.14	0.27	Si + Mg	Mg[b]
385.9	0.02	0	0	0.36	Mg	
389.4	0.1	0.21	0	0.02	Si + Mg	
400.1	0.09	0	0.4	0.1	Mg	
401.1	0.1	0	0.16	0.18	Si + Mg	
405.6	0.18	0	0.1	0.16	Si + Mg	
410.6	0.03	0.29	0.18	0.03	Mg	
424.4	0.15	0	0.19	0.32	Si + Mg	
425.0	0.04	0	0.26	0.3	Mg	
427.1	0.04	0.34	0.03	0.01	Mg	
430.6	0.08	0.37	0.07	0.12	Mg	
448.1	0.2	0	0	0.12	Si + Mg	Mg[c]
454.6	0.02	0	0.21	0.11	Mg	
455.2	0.17	0.16	0.33	0.04	Si + Mg	
462.2	0.1	0.39	0.3	0.12	Si + Mg	
469.4	0.08	0.02	0.24	0.11	Mg	
473.4	0.11	0.36	0	0.03	Si + Mg	
481.7	0.18	0	0.03	0.1	Si + Mg	
483.9	0.03	0	0.03	0.09	Mg	
488.4	0.08	0.02	0.19	0.09	Mg	BM_{SiO3}[b]
498.2	0.18	0.12	0.21	0.05	Si + Mg	
514.0	0.18	0.16	0.02	0.04	Si + Mg	BM_{SiO3}[b]
535.1	0.12	0.27	0.1	0.11	Si + Mg	
543.5	0.08	0	0.09	0.24	Mg	
545.6	0.13	0.13	0	0.01	Si + Mg	
551.0	0.11	0.12	0.08	0.22	Si + Mg	
552.6	0.1	0.2	0.13	0.37	Si + Mg	Si + Mg[b]
556.8	0.04	0	0.25	0.15	Mg	Si + Mg[c]
564.1	0.15	0	0.09	0.02	Si + Mg	
577.9	0.14	0	0.18	0.11	Si + Mg	BM_{SiO3}[c]
586.7	0.19	0.22	0.04	0.15	Si + Mg	BM_{SiO3}[c]
590.3	0.01	0.2	0.07	0.16	Mg	
607.2	0.13	0	0.03	0.14	Si + Mg	BM_{SiO3}[c]
624.6	0.04	0	0.02	0.1	Mg	

Table 3. (continued)

ν_i, cm^{-1}	Si, au	Mg1, au	Mg2, au	Mg3, au	Assignment	
					This Work	Experiment
698.7	0.18	0.12	0.03	0.06	Si + Mg, AS_{SiO3}	Si_2O_7 asymmetric stretch[b]
711.8	0.24	0	0.02	0.01	SS_{SiOSi} + BM_{SiOSi}, SS_{SiO3} + BM_{SiO3}	Si_2O_7 symmetric stretch[c]
785.8	0.22	0	0	0.01	AS_{SiOSi}, SS_{SiO3}	
794	0.2	0.01	0.01	0.01	AS_{SiOSi}, SS_{SiO3}	
828.7	0.07	0	0.04	0.04	AS_{SiOSi}, SS_{SiO3}	SS_{SiO3}[c]
832.6	0.06	0.07	0.05	0.02	AS_{SiOSi}, SS_{SiO3}	SS_{SiO3}[b,c]
871.9	0.18	0.02	0.01	0.03	SS_{SiOSi} + BM_{SiOS}, SS_{SiO3}	
890.6	0.29	0	0.01	0.02	SS_{SiOSi} + BM_{SiOSi}, AS_{SiO3}	
894.7	0.27	0	0	0.01	Lz, AS_{SiO3}	
909.7	0.27	0.02	0.01	0.02	BM_{SiOSi}, AS_{SiO3}	
910.5	0.19	0	0.05	0.03	SS_{SiOSi} + BM_{SiOSi} SS_{SiO3}	SS_{SiO3}[c]
913.5	0.28	0	0.02	0	Lx, AS_{SiO3}	
914.7	0.28	0.01	0	0.01	Lz, AS_{SiO3}	
917.6	0.28	0.01	0.02	0.02	Lx, AS_{SiO3}	AS_{SiO3}[b] Si_2O_7 asymmetric stretch[c]
934.8	0.25	0	0.03	0.03	Ly,AS_{SiO3}	
946.7	0.26	0.05	0	0.03	Ly + AS_{SiOS}, AS_{SiO3}	

[a]Si + Mg, complex vibration involving both SiO_3 and MgO_6 displacement; Mg, vibration predominantly involving MgO_6 displacement, in arbitrary units (au); SS_{SiO3}, SiO_3 symmetric stretch and SS_{SiOSi}, Si-O-Si linkage symmetric stretch; AS_{SiO3}, SiO_3 asymmetric stretch and AS_{SiOSi}, Si-O-Si linkage asymmetric stretch; BM_{SiO3}, SiO_3 bend modes and BM_{SiOSi}, Si-O-Si linkage bend modes; Lx, Si-O-Si linkage libration about x axis; Ly, Si-O-Si linkage libration about y axis; Lz, Si-O-Si linkage libration about z axis. Here x and y axis lie in Si-O-Si plane, x axis lies along Si-Si, z is normal to x and y axis.
[b]From *Williams et al.* [1986].
[c]From *Mernagh and Liu* [1996].

groups in the primitive cell is shown since the atomic displacements of two Si_2O_7 groups are related by symmetry. For example, Raman and infrared modes are even and odd, respectively, under the inversion operation. Some Raman modes have almost the same displacement pattern within a single Si_2O_7 group than the corresponding infrared mode. The difference between them is mainly the even or odd nature of the displacements of one group with respect to the other one.

[9] For the IR mode at 938 cm^{-1}, there are some disagreements in symmetry assignments. *Williams et al.* [1986] assign this mode to a SiO_3 asymmetric stretch. In contrast, *Mernagh and Liu* [1996] attribute this frequency to a Si_2O_7 asymmetric stretch mode. Our results indicate that this vibration is a combination of SiO_3 asymmetric stretch and Si-O-Si bridge libration. Another IR mode at 810 cm^{-1} has been assigned to a SiO_3 symmetric stretch. This is consistent with our results, which indicate that both Si-O-Si asymmetric stretch and SiO_3 symmetric stretch are present in this mode.

[10] *McMillan and Akaogi* [1987] suggested that the 723 and 918 cm^{-1} modes should have A_g symmetry by noticing that these strong peaks are very similar to the major peaks of pyrosilicate akermanite at 661 and 904 cm^{-1}. The modes at 723 and 918 cm^{-1} were also described as a symmetric stretching vibration of the Si-O-Si bridge and of the terminal-SiO_3 group, respectively. Their conjecture is supported by our calculation. The modes nearest to the above frequencies, 711 and 910 cm^{-1}, have A_g symmetry. Both modes include a symmetric stretch vibration of Si-O-Si bridge and of the terminal-SiO_3 group. In addition, the mode at 711 cm^{-1} has a large bending vibration component of the terminal-SiO_3 group as shown in Figure 1. The Raman mode at 813 cm^{-1} has been assigned to a SiO_3 symmetric stretch [*Mernagh and Liu*, 1996], which is also consistent with our results.

[11] By analogy with the bands below about 400 cm^{-1} in olivine, the low-frequency modes of wadsleyite had been assigned by *Williams et al.* [1986] and *Mernagh and Liu* [1996] to vibrations involving predominantly Mg rather than Si displacements. However, our results indicate that most of the low-frequency modes involve both Si and Mg displacements (Table 3). These modes involve complex vibrations of both Si_2O_7 and MgO_6 units. By analogy with olivine the Raman modes at 231 and 443 cm^{-1} and IR modes at 381 cm^{-1} had been assigned in experiments to normal modes involving predominantly MgO_6 displacements. However, they actually are vibrations involving both Si_2O_7 and MgO_6 motions. Therefore our results indicate that analogies between normal mode displacements should not be made on the basis of similarities of phonon frequencies in different structures such as olivine and wadsleyite.

[12] Phonon dispersions at zero and 15 GPa are shown in Figure 2. A previous DFT calculation [*Yu and Wenztcovitch*, 2006] in ringwoodite has shown a phonon gap between 600 and 800 cm^{-1}. For the wadsleyite structure, in this same frequency range, we found a gap plus two sharp peaks located within this gap. The gap differentiates the high-frequency modes involving only vibrations of the Si_2O_7 group, as shown in Figure 1, and other modes involving significant vibration of MgO_6 octahedra. According to the phonon density of states, the band gap is about 141 cm^{-1} at

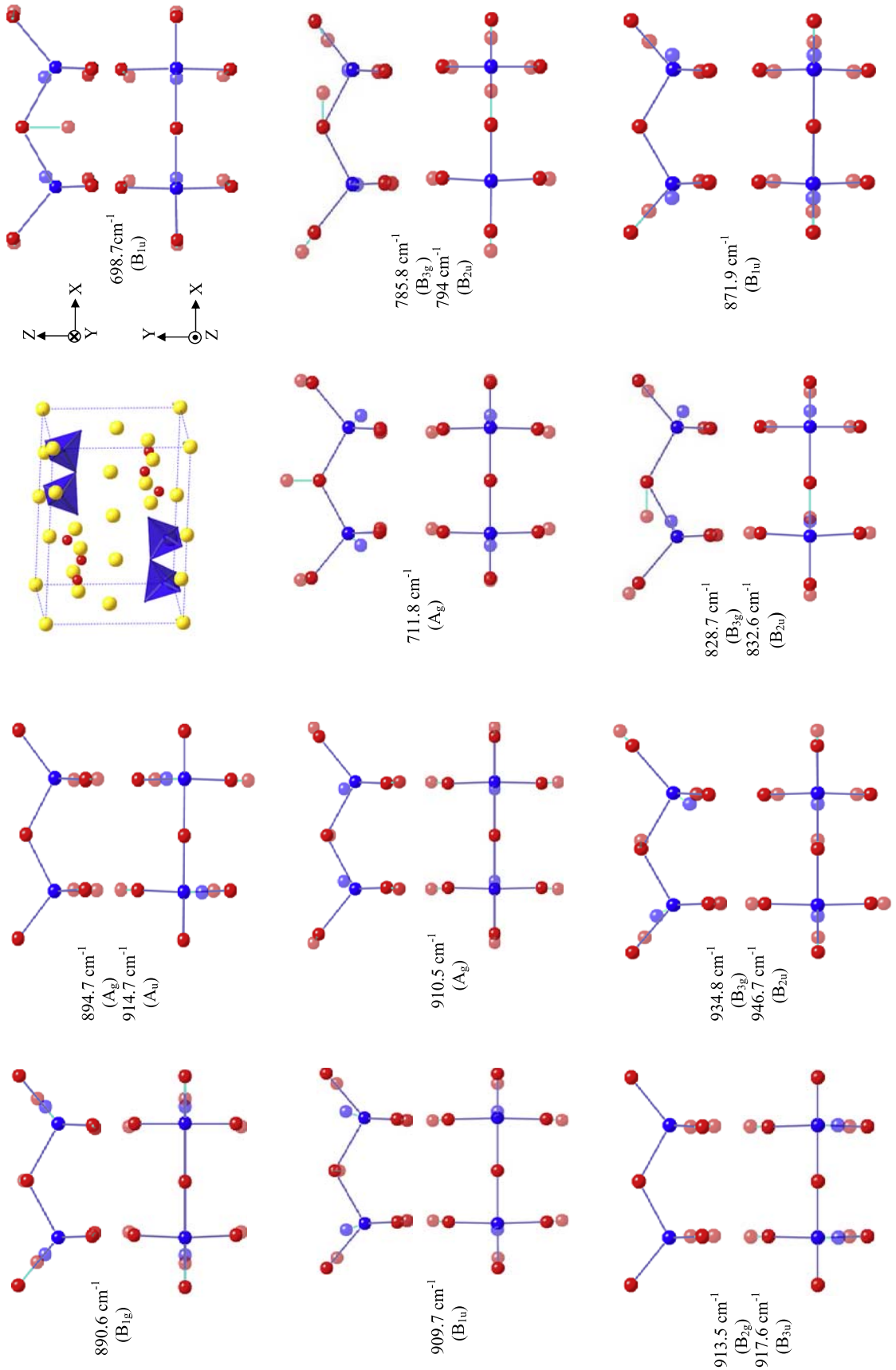

Figure 1. Atomic displacements involved in the high-frequency modes. Magnesium displacements can be almost ignored in these modes. Each primitive cell has two symmetry related Si_2O_7 groups. Raman and infrared modes involve atomic displacements in one group that is plus or minus the atomic displacements of the other group, respectively. Therefore here we only indicate displacements within one Si_2O_7 group. The displacements are shown from the side (along *y* axis) and top (along *z* axis), respectively. Red and blue spheres denote oxygen and silicon, respectively. Displacements are displayed in light color and are amplified uniformly about 4 times for clarity. These modes are identified by their frequencies and symmetries.

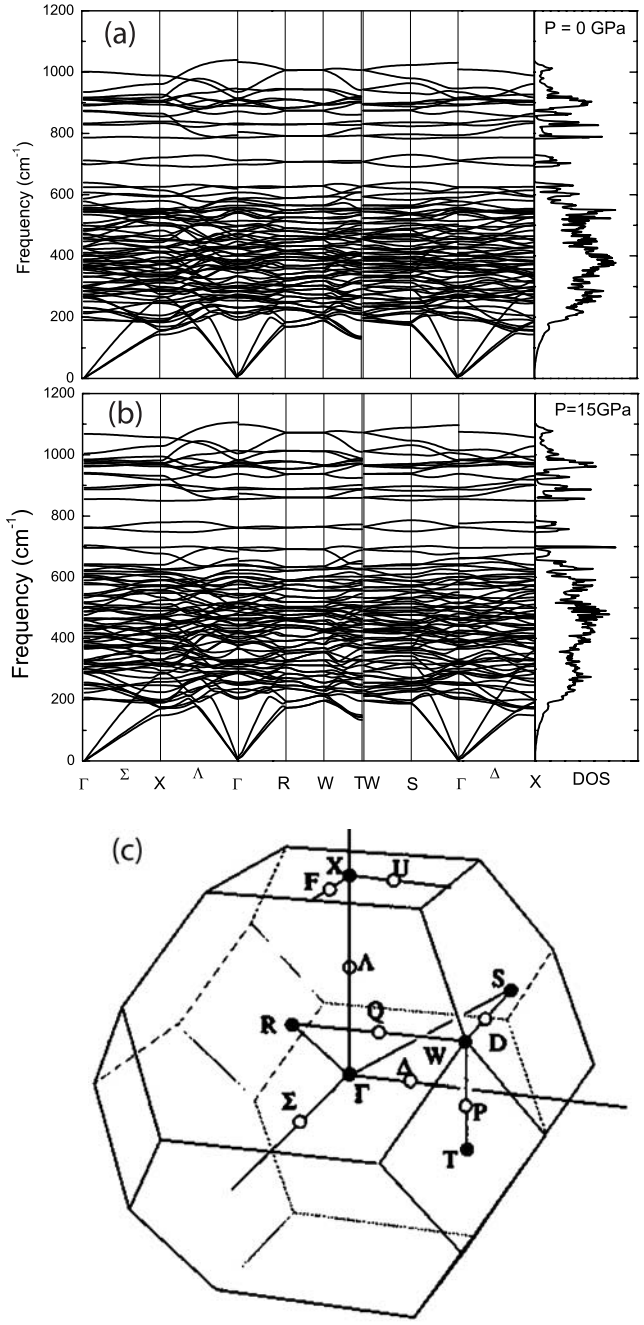

Figure 2. Phonon dispersions and densities of states at (a) 0 GPa, (b) 15 GPa, and (c) the first Brillouin zone of the *Immm* space group.

0 GPa and 147 cm^{-1} at 15 GPa, showing a small tendency to increase with pressure.

4. Thermodynamics Properties

[13] The Helmholtz free energy in the quasi-harmonic approximation (QHA) is given by

$$F(V,T) = U_0(V) + \frac{1}{2}\sum_{q,j}\hbar\omega_j(q,V) + k_BT\sum_{q,j} \cdot \ln\{1-\exp[-\hbar\omega_j(q,V)/k_BT]\}, \quad (2)$$

where the first, second, and third terms are the static internal, zero point, and vibrational energy contributions, respectively. The converged summation is performed on a 9 × 9 × 9 regular q mesh in the first Brillouin zone.

[14] The calculated Helmholtz free energies versus volume were fitted by isothermal third-order finite strain equations of state. The resulting pressure-volume relations are described by a third-order Birch-Murnaghan equation of states (EOS). The temperature dependence of the three EOS parameters are fitted to a polynomial and listed in Table 4. Equations of states at various temperatures are shown in Figure 3. The volumes given by LDA static calculations are smaller than the experimental values at room temperature. Zero point motion and room temperature effects increase V_0 by 1.3% and decrease K_{T0} by 5.2% from their LDA static values. The 300 K isotherm is in excellent agreement with the experimental data by *Hazen et al.* [2000] and is also very consistent with the data by *Fei et al.* [1992] on 16% Fe wadsleyite if the effect of iron is taken into account (volume increase by 1%). The three lattice constants at room temperature were determined using the statically constrained quasi-harmonic approximation [*Carrier et al.*, 2007]. According to this approximation, crystal structure and phonon frequencies depend on volume alone. Their dependence on pressure and temperature is indirect through volumetric effects only. It can be seen that the lattice parameters decrease uniformly with increasing pressure and agree fairly well with experimental observations [*Hazen et al.*, 2000] (Figure 4). The calculated thermodynamic parameters at ambient conditions are shown in Table 5 and are in good agreement with the experimental data. Similarly, our result at 1000 K of V_0 = 552.9 $Å^3$ compares very well with the experimental data of 549.6 $Å^3$ [*Suzuki et al.*, 1980].

[15] As shown in Figure 5, the thermal expansivity $\alpha = (1/V)\,(\partial V/\partial T)_P$ is in good agreement with the experimental value [*Watanabe*, 1982] at low temperatures; α from experimental observations shows the linear temperature dependence at high temperatures. In contrast, α from QHA calculations deviates from this linear behavior at a certain temperature and increases relatively quickly compared to the experimental data. This type of deviation is typical of the QHA [*Karki et al.*, 1999] and points to an upper temperature limit of validity of this approximation [*Wentzcovitch et al.*, 2004]. This limit can be defined by the position of the inflection point in α, and in Figure 5 this point separates full and dashed lines; α decreases quickly with pressure. The effect of temperature on α becomes less and less pronounced and the linear temperature behavior extends to very high temperatures at high pressures. Therefore the upper temperature limit of validity of the QHA increases rapidly with pressure.

Table 4. Coefficients of Polynomial Fit for Three EOS Parameters of Wadsleyite[a]

	T^0	T^1	T^2	T^3	T^4
V_0	1818.8110	18.4249	38.8299	−13.1094	2.1534
K_{T0}	170.9010	−15.9152	−9.95773	3.7505	−0.5516
K_{T0}'	4.3556	0.2757	−0.0110	0.0085	6.2887×10^{-4}

[a]Temperature in units of 1000 K.

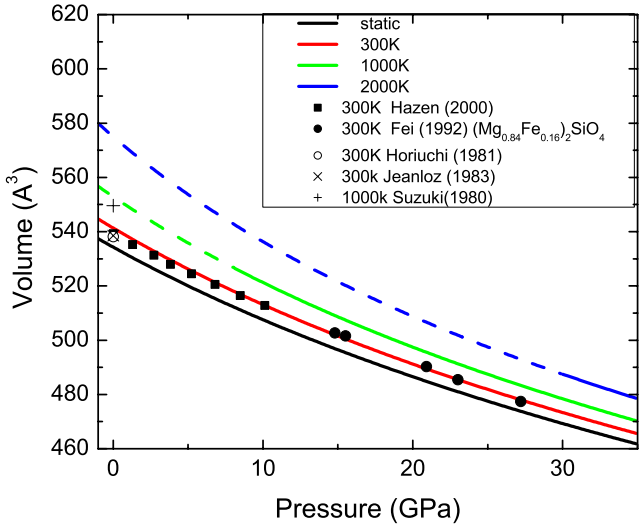

Figure 3. PVT relations in wadsleyite. Dashed lines correspond to the conditions where the validity of QHA is questionable [*Wentzcovitch et al.*, 2004] (see text). Hazen (2000) is *Hazen et al.* [2000], Fei (1992) is *Fei et al.* [1992], Horiuchi (1981) is *Horiuchi and Sawamoto* [1981], Jeanloz (1983) is *Jeanloz and Thompson* [1983], Suzuki (1980) is *Suzuki et al.* [1980].

[16] The thermal Grüneisen parameter is shown in Figure 6. This parameter is useful in calculating the thermal pressure and can be expressed as $\gamma_{th} = \alpha K_T V/C_V$, where K_T and C_V are isothermal bulk modulus and heat capacity at constant volume, respectively. We find that the low-temperature dependence of γ_{th} at low pressure is completely different from that at high pressure. At zero pressure, γ_{th} shows a nonmonotonic behavior. It has a peak at T = 160 K, decreases with temperature up to T = 600 K, and then increases with temperature. A similar decrease has been observed experimentally [*Watanabe*, 1982]. Our calculated mean value of γ_{th} = 1.26 in the temperature range between 350 K and 700 K compares well with *Watanabe*'s [1982] result, 1.29 ± 0.02. At 10 GPa and higher pressures, γ_{th} increases monotonically with temperature and tends to nearly a constant with a very small linear T dependence at high temperatures; γ_{th} decreases with increasing pressure

Table 5. Thermodynamic Parameters of Wadsleyite at Ambient Conditions

	Calculated	Experimental
V_0, Å^3	541.35, 536.95[a], 535.1[b]	539.26(9)[c], 535.30(27)[d], 538.13[e]
K_{T0}, GPa	165.7, 169.7[a] 169.2[b]	172(3)[c], 160(3)[d]
K_{S0}, GPa	167.1	170(2)[f], 163[g], 174[h], 170[i]
$\partial K_T/\partial P$	4.44, 4.15[a], 4.53[b]	6.3(7)[c], 4.0[d]
$\partial K_S/\partial P$	4.41	4.3(2)[f], 4.8[g], 4.24(10)[i]
α, 10^{-5} K^{-1}	2.21	2.06[j]
γ_{th}	1.28	1.26[j],1.327[k]
C_p, J mol^{-1} K^{-1}	118.1	114.14[l]
S, J mol^{-1} K^{-1}	88.67	85.87[m], 85.52[n], 87.32[o]

[a] *Matsui* [1999].
[b] *Kiefer et al.* [2001].
[c] *Hazen et al.* [2000].
[d] *Hazen et al.* [1990].
[e] *Horiuchi and Sawamoto* [1981].
[f] *Zha et al.* [1997].
[g] *Gwanmesia et al.* [1990].
[h] *Sawamoto et al.* [1984].
[i] *Li et al.* [1996].
[j] *Suzuki et al.* [1980].
[k] *Watanabe* [1982].
[l] *Ashida et al.* [1987].
[m] *Chopelas* [1991].
[n] *Price et al.* [1987].
[o] *Akaogi et al.* [1984].

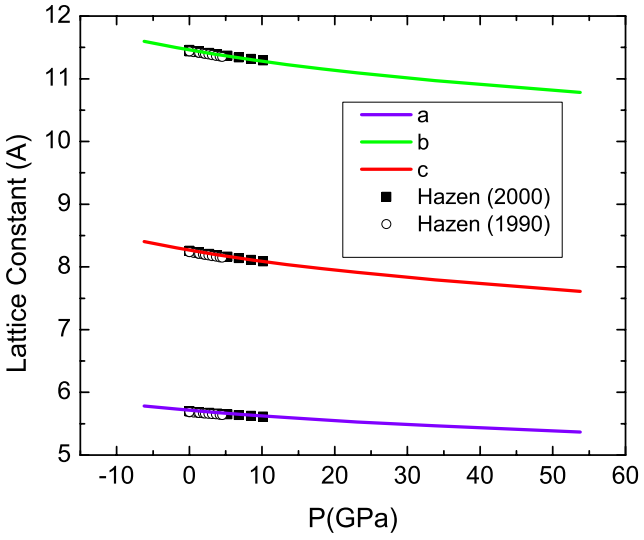

Figure 4. Pressure dependence of the lattice constant of wadsleyite at room temperature. Our results at room temperature were obtained using the statically constrained QHA [*Carrier et al.*, 2007]. Hazen (1990) is *Hazen et al.* [1990], and Hazen (2000) is *Hazen et al.* [2000].

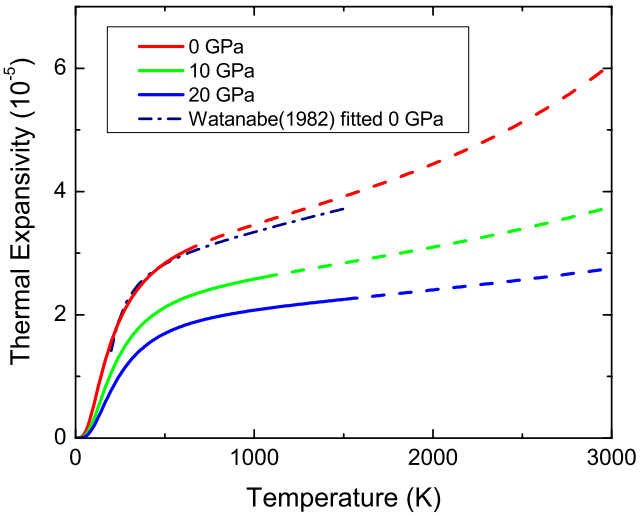

Figure 5. Thermal expansivity of wadsleyite at various pressures. Dashed lines have the same meaning as in Figure 3.

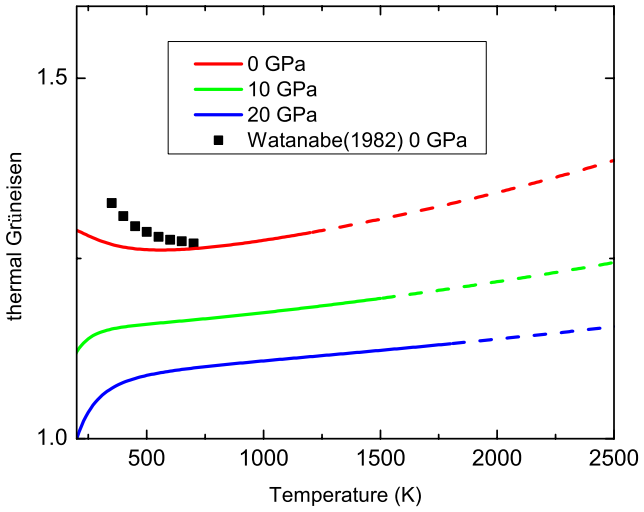

Figure 6. Thermal Grüneisen parameter at various pressures. Dashed lines have the same meaning as in Figure 3.

and varies from 1.27 to 1.06 between 0 and 20 GPa at room temperature.

[17] The heat capacity at constant pressure, C_P, and volume, C_V, are related by $C_P = (1 + a\gamma_{th}T)C_V$. At zero pressure, C_P is consistent with the experimental observation [*Ashida et al.*, 1987] at low temperatures but begins to deviate from experimental values beyond 500 K (Figure 7). The calculated C_V is closer to *Chopelas*' [1991] experimental data and a little larger than C_V from lattice dynamic calculations using interatomic potentials [*Price et al.*, 1987] at high temperatures. As shown in Figure 8, the calculated entropy is also in good agreement with experimental estimates at zero pressure [*Chopelas*, 1991; *Akaogi et al.*, 1984] and lattice dynamic calculations using interatomic potentials [*Price et al.*, 1987]. Unlike α and C_P, which vary linearly with temperature at high pressures, the temperature dependence of the entropy is almost pressure-insensitive.

[18] Figure 9 shows the temperature dependence of the adiabatic bulk modulus (K_S) at various pressures. The temperature dependence of K_S is small at low temperatures but becomes linearly dependent with temperature above about 1500 K. For example, $(\partial K_S/\partial T)_P$ at 0 GPa changes from -0.0152 GPa K^{-1} at 300 K to -0.019 GPa K^{-1} at 1000 K. $(\partial K_S/\partial T)_P$ is also quite sensitive to pressure. For example, at room temperature, $(\partial K_S/\partial T)_P$ changes from -0.0152 GPa K^{-1} at 0 GPa to -0.0114 GPa K^{-1} at 20 GPa, a change of ~25%. This indicates that one should be careful and not extrapolate measurements of $(\partial K_S/\partial T)_P$ obtained at ambient conditions to transition zone pressures and temperatures.

[19] Our calculated zero pressure value of $(\partial K_S/\partial_T)_P$ -0.0152 GPa K^{-1}, agrees well with the experimental value of -0.016 GPa K^{-1} for $(Mg_{0.91}Fe_{0.09})_2SiO_4$ determined by *Katsura et al.* [2001]. However, these values are somewhat different from -0.012 GPa K^{-1}, the value determined for the end-member Mg_2SiO_4 by *Li et al.* [1998] at high pressures. The pressure dependence of $(\partial K_S/\partial_T)_P$ should contribute at least in part to this discrepancy. The larger value (smaller in magnitude) of $(\partial K_S/\partial_T)_P$ by *Li et al.* [1998] is consistent with the pressure effect on $(\partial K_S/\partial_T)_P$. Our calculated $(\partial K_S/\partial_T)_P$ should be reliable since our method was shown to reproduce $(\partial K_S/\partial_T)_P$ very well for

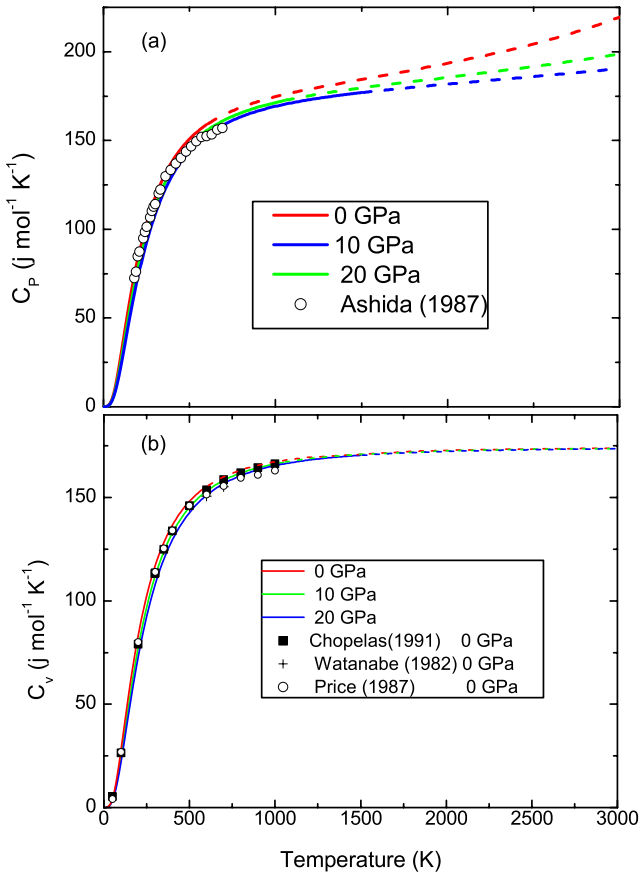

Figure 7. Heat capacity at (a) constant pressure and (b) constant volume at various pressures. Dashed lines have the same meaning as in Figure 3. Ashida (1987) is *Ashida et al.* [1987], and Price (1987) is *Price et al.* [1987].

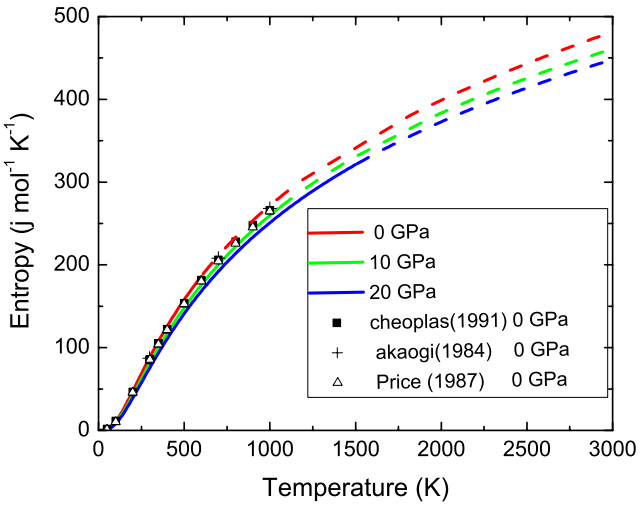

Figure 8. Temperature dependence of entropy at various pressures. Dashed lines have the same meaning as in Figure 3. Akaogi (1984) is *Akaogi et al.* [1984], and Price (1987) is *Price et al.* [1987].

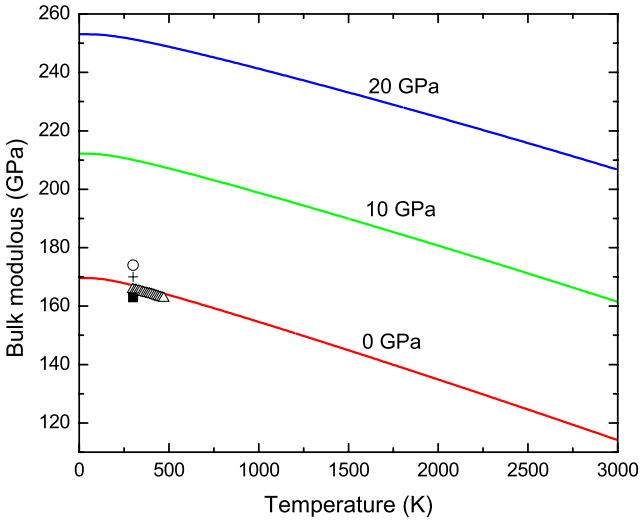

Figure 9. Temperature dependence of adiabatic bulk modulus at various pressures. Experimental data are denoted by open circles [*Sawamoto et al.*, 1984], crosses [*Li et al.*, 1996], open triangles [*Katsura et al.*, 2001], and solid squares [*Gwanmesia et al.*, 1990], respectively.

other two phases of Mg_2SiO_4 [*Yu and Wentzcovitch*, 2006; *Li et al.*, 2007]. Besides, the consistence between our result and *Katsura et al.*'s [2001] results suggest that iron has little effect on $(\partial K_S/\partial T)_P$. This conclusion is also consistent with the experimental observation that there are no significant differences in the temperature derivative of the bulk modulus of iron-bearing olivine and of the end-member forsterite [*Isaak*, 1992]. However, iron content will inevitably affect the bulk modulus. For example, the bulk modulus of iron-bearing wadsleyite by *Katsura et al.* [2001] is slightly lower than those obtained by most experiments on the end-member wadsleyite [*Li et al.*, 1996; *Zha et al.*, 1997; *Sawamoto et al.*, 1984]. Therefore iron concentration should still affect a little $(\partial K_S/\partial T)_P$.

[20] The transition zone is believed to have considerable amounts of water besides iron. Wadsleyite can incorporate up to 3.3 wt % H_20 in its structure. In contrast to the incorporation of iron, the incorporation of hydrogen in wadsleyite produces vacancies and hence always weakens its strength. The adiabatic bulk modulus of wadsleyite decreases about 15 GPa after incorporating 2.5 wt % H [*Zha et al.*, 1997; *Yusa and Inoue*, 1997], far more than the effect of iron on the bulk modulus. Besides, vacancies concentration usually changes with temperature. This complicates the effect of hydrogen on *Ks* and $(\partial K_S/\partial T)_P$.

5. Conclusion

[21] The vibrational and thermodynamic properties of wadsleyite have been investigated using density functional perturbation theory to obtain vibrational density of states and the quasi-harmonic approximation to compute free energies. Both the frequencies and their dependence on pressure are in good agreement with those observed by Raman and infrared measurements. Our calculations provide several vibrational properties such as mode symmetries and atomic displacement patterns, which are still unknown for most modes. The highest 15 modes consist mainly of vibrations of the Si_2O_7 unit keeping magnesium nearly stationary. These modes have smaller Grüneisen parameters than the lower-frequency modes involving the vibration of MgO_6 octahedra. This is consistent with experimental results and indicates that the Si_2O_7 group is less compressive than the MgO_6 group. Thermodynamic quantities of interest have been derived and are in good agreement with various sets of the experimental data. Our calculations provide excellent thermodynamic properties of this important mineral over the large pressure-temperature regime relevant for the Earth. The contributions of zero motion and 300 K to elastic properties are significant (~5.2% in the bulk modulus); therefore one should be careful in comparing athermal (static) results with experimental data at ambient conditions.

[22] **Acknowledgments.** Calculations were performed with the Quantum ESPRESSO package (http://www.pwscf.org). Work supported by NSF/EAR 0230319, 0635990, and NSF/ITR 0428774 (VLab).

References

Akaogi, M., N. L. Ross, P. McMillan, and A. Navrotsky (1984), The Mg_2SiO_4 polymorphs (olivine, modified spinel and spinel)—Thermodynamic properties from oxide melt solution calorimetry, phase relations, and models of lattice vibrations, *Am. Mineral.*, *69*, 499–512.

Ashida, T., S. Kume, and E. Ito (1987), *High-Pressure Research in Mineral Physics*, *Geophys. Monogr. Ser.*, vol. 39, edited by M. H. Manghnani and Y. Syono, 269 pp., AGU, Washington, D. C.

Baroni, S., S. de Gironcoli, A. Dal Corso, and P. Giannozzi (2001), Phonons and related crystal properties from density-functional perturbation theory, *Rev. Mod. Phys.*, *73*, 515–562.

Carrier, P., R. M. Wentzcovitch, and J. Tsuchiya (2007), Predictions of crystal structures at high pressures and temperatures under the quasiharmonic approximation, *Phys. Rev. B*, *76*, 064116.

Chopelas, A. (1991), Thermal properties of β-Mg_2SiO_4 at mantle pressures derived from vibrational spectroscopy: Implications for the mantle at 400 km depth, *J. Geophys. Res.*, *96*, 11,817–11,829.

Chopelas, A., R. Boehler, and T. Ko (1994), Thermodynamics and behavior of γ-Mg_2SiO_4 at high pressure: Implications for Mg_2SiO_4 phase equilibrium, *Phys. Chem. Miner.*, 21,351–21,359.

Cynn, H., and A. M. Hofmeister (1994), High-pressure IR spectras of lattice modes and OH vibrations in Fe-bearing wadsleyite, *J. Geophys. Res.*, *99*, 17,717–17,727.

Fei, Y., H. Mao, J. Shu, G. Parthasarathy, W. A. Bassett, and J. Ko (1992), Simultaneous high-P, high-T X ray diffraction study of beta-$(Mg,Fe)_2SiO_4$ to 26 GPa and 900 K, *J. Geophys. Res.*, *97*, 4489–4495.

Gwanmesia, G. D., S. Rigden, I. Jackson, and R. C. Liebermann (1990), Pressure dependence of elastic wave velocity for β-Mg2SiO4 and the composition of the Earth's mantle, *Science*, *250*, 794–797.

Hazen, R. M. (1976), Effects of temperature and pressure on the crystal structure of forsterite, *Am. Mineral.*, *61*, 1280–1293.

Hazen, R. M., J. M. Zhang, and J. Ko (1990), Effects of Fe/Mg on the compressibility of synthetic wadsleyite: β-$(Mg_{1-x}Fex)_2SiO_4$($x \leq 0.25$), *Phys. Chem. Miner.*, *17*, 416–419.

Hazen, R. M., M. R. Weinberger, H. Yang, and C. T. Prewitt (2000), Comparative high-pressure crystal chemistry of wadsleyite, beta-$(Mg_{1-x}Fe_x)_2SiO_4$, with x = 0 and 0.25, *Am. Mineral.*, *85*, 770–777.

Horiuchi, H., and H. Sawamoto (1981), β-$(Mg_{1-x}Fe_x)_2SiO_4$: Single-crystal X-ray diffraction study, *Am. Mineral.*, *66*, 568–575.

Inoue, T., H. Yurimoto, and Y. Kudoh (1995), Hydrous modified spinel $Mg_{1.75}SiH_{0.5}O_4$: A new water reservoir in the mantle transition region, *Geophys. Res. Lett.*, *22*, 117–120.

Isaak, D. G. (1992), High-temperature elasticity of iron-bearing olivines, *J. Geophys. Res.*, *97*, 1871–1885.

Jacobsen, S. D., S. Demouchy, D. J. Frost, T. Boffa Ballaran, and J. Kung (2005), A systematic study of OH in hydrous wadsleyite from polarized FTIR spectroscopy and single-crystal X-ray diffraction: Oxygen sites for hydrogen storage in Earth's interior, *Am. Mineral.*, *90*, 61–70.

Jeanloz, R., and A. B. Thompson (1983), Phase transitions and mantle discontinuities, *Rev. Geophys.*, *21*, 51–74.

Karki, B. B., and R. M. Wentzcovitch (2003), Vibrational and quasiharmonic thermal properties of CaO under pressure, *Phys. Rev. B*, *68*, 224,304.

Karki, B. B., R. M. Wentzcovitch, S. De Gironcoli, and S. Baroni (1999), High-pressure lattice dynamics and thermoelasticity of MgO, *Phys. Rev. B*, *61*, 8793–8800.

Katsura, T., N. Mayama, K. Shouno, M. Sakai, A. Yoneda, and I. Suzuki (2001), Temperature derivatives of elastic moduli of $(Mg_{0.91}Fe_{0.09})_2SiO_4$ modified spinel, *Phys. Earth Planet. Inter.*, *124*, 163–166.

Kiefer, B., L. Stixrude, J. Hafner, and G. Kresse (2001), Structure and elasticity of wadsleyite at high pressures, *Am. Mineral.*, *86*, 1387–1395.

Kleppe, A. K., A. P. Jephcoat, H. Olijnyk, A. E. Slesinger, S. C. Kohn, and B. J. Wood (2001), Raman spectroscopic study of hydrous wadsleyite (β-Mg_2SiO_4) to 50 GPa, *Phys. Chem. Miner.*, *28*, 232–241.

Kohlstedt, D. L., H. Keppler, and D. C. Rubie (1996), Solubility of water in the alpha, beta and gamma phases of $(MgFe)_2SiO_4$, *Contrib. Mineral. Petrol.*, *123*, 345–357.

Kohn, S. C., R. A. Brooker, D. J. Frost, A. E. Slesinger, and B. J. Wood (2002), Ordering of hydroxyl defects in hydrous wadsleyite (β-Mg_2SiO_4), *Am. Mineral.*, *87*, 293–301.

Kudoh, Y., T. Inoue, and H. Arashi (1996), Structure and crystal chemistry of hydrous wadsleyite, $Mg_{1.75}SiH_{0.5}O_4$: possible hydrous magnesium silicate in the mantle transition zone, *Phys. Chem. Miner.*, *23*, 461–469.

Li, B., G. D. Gwanmesia, and R. C. Liebermann (1996), Sound velocities of olivine and beta polymorphs of Mg_2SiO_4 at Earth's transition zone pressures, *Geophys. Res. Lett.*, *23*, 2259–2262.

Li, B., R. C. Liebermann, and D. J. Weidner (1998), Elastic moduli of wadsleyite (β-Mg_2SiO_4) to 7 gigapascals and 873 kelvin, *Science*, *281*, 675–677.

Li, L., R. M. Wentzcovitch, D. J. Weidner, and C. R. S. Da Silva (2007), Vibrational and thermodynamic properties of forsterite at mantle conditions, *J. Geophys. Res.*, *112*, B05206, doi:10.1029/2006JB004546.

Matsui, M. (1999), Computer simulation of the Mg_2SiO_4 phases with application to the 410 km seismic discontinuity, *Phys. Earth. Planet. Inter.*, *116*, 9–18.

McMillan, P. F., and M. Akaogi (1987), Raman spectra of β-Mg_2SiO_4(modified spinel) and γ-Mg_2SiO_4(spinel), *Am. Mineral.*, *72*, 361–364.

Mernagh, T. P., and L. Liu (1996), Raman and infrared spectra of hydrous β-Mg_2SiO_4, *Can. Mineral.*, *34*, 1233–1240.

Ohtani, E., and K. D. Litasov (2006), The effect of water on mantle phase transitions, in *Water in Nominally Anhydrous Minerals*, *Rev. Mineral. Geochem.*, vol. 62, edited by H. Keppler and J. R. Smyth, pp. 397–419, Mineral. Soc. of Am., Washington, D. C.

Perdew, J. P., and A. Zunger (1981), Self-interaction correction to density-functional approximations for many-electron systems, *Phys. Rev. B*, *23*, 5048–5079.

Price, G. D., S. C. Parker, and M. Leslie (1987), The lattice dynamics and thermodynamics of the Mg_2SiO_4 polymorphs, *Phys. Chem. Miner.*, *15*, 181–190.

Reynard, B., F. Takir, F. Guyot, G. D. Gwanmesia, R. C. Liebermann, and P. Gillett (1996), High-temperature Raman spectroscopic and X-ray diffraction study of β-Mg_2SiO_4: Insights into its high-temperature thermodynamic properties and the β- to α- phase-transformation mechanism and kinetics, *Am. Mineral.*, *81*, 585–594.

Ringwood, A. E. (1975), Composition and Petrology of the Earth's Mantle, McGraw-Hill, New York. pp. 618.

Sawamoto, H., D. J. Weidner, S. Sasaki, and M. Kumazawa (1984), Single-crystal elastic properties of the modified spinel (beta) phase of magnesium orthosilicate, *Science*, *224*, 749–751.

Smyth, J. R. (1987), β-Mg_2SiO4: A potential host for water in the mantle?, *Am. Mineral.*, *72*, 1051–1055.

Smyth, J. R. (1994), A crystallographic model for hydrous wadsleyite (β-Mg2SiO4), An ocean in the Earth's interior, *Am. Mineral.*, *79*, 1021–1025.

Suzuki, I., E. Ohtani, and M. Kumazawa (1980), Thermal expansion of modified spinel, β-Mg_2SiO_4, *J. Phys. Earth*, *28*, 273–280.

Troullier, N., and J. L. Martins (1991), Efficient pseudopotentials for plane-wave calculations, *Phys. Rev. B*, *43*, 1993–2006.

Watanabe, H. (1982), Thermochemical properties of synthetic high-pressure compounds relevant to the Earth's mantle, in *High-Pressure Research in Geophysics*, *Adv. Earth Planet. Sci.*, vol. 12, edited by S. Akimoto and M. H. Manghani, pp. 441–464, Cent. for Acad. Publ., Jpn., Tokyo.

Wentzcovitch, R. M. (1993), Invariant molecular dynamics approach to structural phase transitions, *Phys. Rev. B*, *44*, 2358–2361.

Wentzcovitch, R. M., B. B. Karki, M. Cococcioni, and S. de Gironcoli (2004), Thermoelastic properties of $MgSiO_3$–perovskite: Insights on the nature of the Earth's lower mantle, *Phys. Rev. Lett.*, *92*, 018501.

Williams, Q., R. Jeanloz, and M. Akaogi (1986), Infrared vibrational spectra of beta-phase Mg_2SiO_4 and Co_2SiO_4 to pressures of 27 GPa, *Phys. Chem. Miner.*, *13*, 141–145.

Yu, Y. G., and R. M. Wentzcovitch (2006), Density functional study of vibrational and thermodynamic properties of ringwoodite, *J. Geophys. Res.*, *111*, B12202, doi:10.1029/2006JB004282.

Yusa, H., and T. Inoue (1997), Compressibility of hydrous wadsleyite (β-phase) in Mg_2SiO_4 by high pressure X-ray diffraction, *Geophys. Res. Lett.*, *24*, 1831–1834.

Zha, C., T. S. Duffy, H. Mao, R. T. Downs, R. J. Hemley, and D. J. Weidner (1997), Single-crystal elasticity of β-Mg_2SiO_4 to the pressure of the 410 km seismic discontinuity in the Earth's mantle, *Earth Planet. Sci. Lett.*, *147*, E9–E15.

R. M. Wentzcovitch and Z. Wu, Department of Chemical Engineering and Materials Science and Minnesota Supercomputing Institute, University of Minnesota-Twin Cities, Minneapolis, MN 55455, USA. (wuzq@cems.umn.edu)